Modification and Numerical Modelling of Dense Plasma Focus Device

Rachel Reuben

Thesis submitted to the Faculty of the

Virginia Polytechnic Institute and State University

in partial fulfillment of the requirements for the degree of

Master of Science

in

Aerospace Engineering

Colin S. Adams, Chair

Scott England

Mark Pierson

August 8, 2024

Blacksburg, Virginia

Keywords: Dense plasma focus, neutron production, pulsed power

Modification and Numerical Modelling of Dense Plasma Focus Device

Rachel Reuben

ABSTRACT

A dense plasma focus device (DPF) is a pulsed power device that generates high energy particles, neutrons and X-rays through rapid compression of the plasma. The presented research investigates the modification of the DPF and use of numerical modelling to predict the neutron yield. The DPF is a 1kJ device that uses a 1.3 uF capacitor and operated at 40 kV pulse. Spark gap switch SG181-C is integrated into the driver circuit to handle high current operations. Bus work is designed and modeled to predict the current waveform generated by the modified DPF. The control system is designed to be suitable for automation using DAQ and LabVIEW. Radial trajectories during pinch formation are analyzed using a numerical model. Two numerical models are used to investigate how neutron yield varies with pressure, pinch current and pinch duration. The modified DPF showed the neutron scaling to be fourth power of the pinch current.

Modification and Numerical Modelling of Dense Plasma Focus Device

Rachel Reuben

GENERAL AUDIENCE ABSTRACT

Nuclear fusion has been researched widely for decades as a solution to meet the demand of increasing energy needs. Controlled fusion reactions has been the main challenge to achieve this and various approaches have been explored using different confinement methods. All the approaches have advantages with different challenges. One approach being explored is the dense plasma focus (DPF) device, which uses electrical discharges to create a dense 'pinch' of plasma where fusion reactions occur when operated in deuterium fuel gas. Recent DPF experiments have shown that kJ range devices are capable of generating neutrons and intense radiation. This research gives an overview of the DPF with energy of 1 kJ range. The DPF is modelled to predict the pinch formation parameters. The model also predicts how neutron yield varies with operating pressure, pinch current and duration.

Acknowledgments

I would like to express my deepest gratitude to my advisor Dr. Colin Adams, for the opportunity to conduct research in what I am interested in. His knowledge and insights were instrumental in the completion of this thesis. I am also thankful to my committee members Dr. Scott England and Dr. Mark Pierson for reviewing my thesis. My sincere thanks to Dr. Daniel Weber, for his advice and knowledge which significantly contributed to the quality of my research. I am also grateful to Trenton Brewer for his guidance and assistance during critical moments of my study. This research would not have been possible without the support of those closest to me. I want to thank my parents, whose unwavering support and encouragement pushed me through the hard times. Lastly, I am grateful to my friends who encouraged and motivated me throughout this journey. Your belief in me made all the difference.

Contents

List of Figures

List of Tables

List of Abbreviations

T_0	stagnant gas temperature
ξ_A	axial sweep efficiency
k	boltzmann constant
r_1	inner electrode radius
r_1	outer electrode radius
a	anode radius
$B0$	magnetic field
E	energy
I_0	pinch current
J_z	axial current density
V_s	velocity of plasma sheath
Ar	argon
D-D	deuterium - deuterium
DAQ	data acquisition system
DPF	dense plasma focus
H	hydrogen

He	helium
HV	high voltage
ICF	inertial confinement fusion
Kr	krypton
N2	nitrogen
NIF	national ignition facility
T	tritium
JET	joint european torous

Chapter 1

Introduction

The dense plasma focus device (DPF) is a coaxial plasma gun based on the pinch phenomenon that causes rapid heating and compression of a plasma sheath into a plasmoid. The gas within the plasmoid generates substantial radiation such as high-energy X-rays, ions, electrons, and with deuterium as fuel, neutrons with densities reaching several 10^{20} cm^{-3} and temperatures attaining few keV during the pulses that last a few nanoseconds for small devices and microseconds for large devices. Plasma focus devices are compact and simple and were first developed in the 1960's. DPFs have been studied extensively in a wide range of energies from MJ to sub kJ devices with the aim of increasing neutron production. Experiments showed that DPFs create hot, dense plasma but neutron production scales much slower than needed for energy production. DPFs also have various important applications such as nuclear material detection, X-ray lithography and medical applications. Recently, research efforts have been focused on increasing neutron yield and understanding the physical mechanisms of pinch formations using unconventional geometries and different gas fuels.

1.1 Fusion Background

To fuse particles, they must overcome the Coulomb barrier. For this the reacting charged particles must be close together enough for sufficient time period. These particles must have kinetic energies of several keV to overcome the repulsive forces. A viable approach

to controlled fusion is still being pursued by studying various confinement methods, each with its own advantages. Two primary approaches are magnetic confinement and inertial confinement. Magnetic confinement, demonstrated by the tokamak concept (e.g., JET) [4], utilizes strong magnetic fields for long duration of confinement and heating. While JET holds a fusion yield record, it hasn't reached breakeven due to size limitations [5]. Inertial confinement fusion (ICF) involves focusing high-energy lasers on a fuel capsule, creating an implosion that heats the core to fusion conditions. The National Ignition Facility (NIF) is the largest ICF facility in the world which has recently achieved fusion energy gain Q of 3.5 MJ [6]. Z Pinch devices are a compact configuration and the mechanism consists of strong electric currents to generate magnetic field to compress the plasma enough for fusion reaction [7].

1.2 Dense Plasma Focus

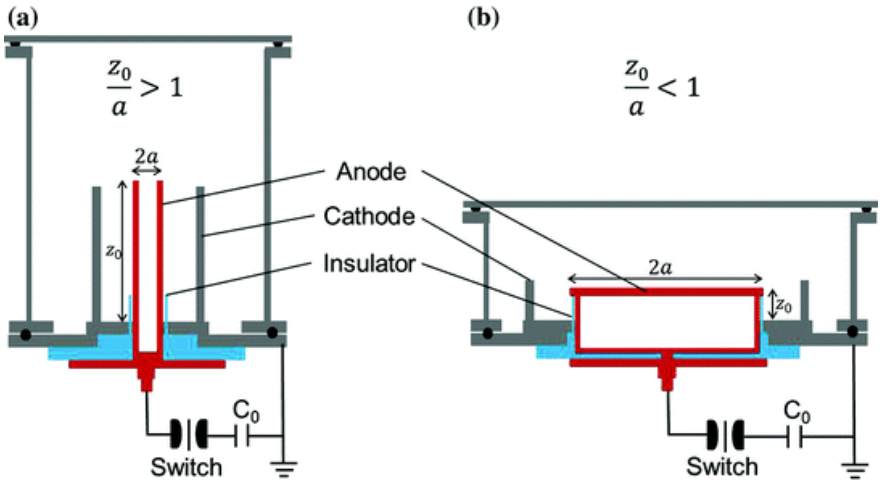

Figure 1.1: Schematic of DPF device showing major components varying in the aspect ratio developed by (a) Mather and (b) Filipov Image credits:[1]

Bennett proposed in 1934 that a stream of ions and electrons could be confined by their own magnetic field [8]. At the start of controlled fusion research (CFR) in the early 1950s, this was

the only theoretical approach for containing a hot plasma. Magnetohydrodynamics (MHD), a theory primarily used in astrophysics, was the only method to study this concept [9]. The analysis from MHD showed that the instability growth caused by the pressure equilibrium between the magnetic field caused plasma loss and led the controlled fusion research to configurations with toroidal topology. Dense Plasma Focus (DPF) interest grew in the 60's and 70's as studies by Mather [10] and Filipov [11] showed that they could produce neutron yields in 10^{10} neutrons/pulse. Their devices differed in the aspect ratio (electrode length divided by diameter). The scaling of neutron as fourth power of current was mentioned first by Mather and PF devices grew interest as a candidate for CFR [12]. The interest decreased when it was discovered that the primary mechanism for neutron production was not due to thermal plasma. The failure of scaling of some devices and loss of funding caused a gap in the theoretical basis for PF physics. Later the research shifted towards alternative uses of DPFs, both to understand the scaling issues and to demonstrate their application as neutron sources. In the 1990s, interest was revived when Sing Lee initiated a project to develop a simple, low-cost plasma focus facility.

The DPF is a simple compact device with geometry consisting of two coaxial electrodes separated by a insulator sleeve which is enclosed in vacuum chamber filled with fuel gas. The capacitors discharge a pulse of high voltage current, the gas ionizes and breaks down at the insulator sleeve, and plasma sheath runs radially from the insulator to the electrode. Then it accelerates axially and reaches the edges of the electrodes and gets magnetically compressed, and forms a plasmoid of very high density 10^{20} cm^{-3} and energy approximately $1 - 10 \times 10^{10}$ J/m^3 [13]. The design of DPF has been extensively researched, with investigations into scaling laws and devices spanning from kJ to MJ energy [14]. Soto's work has contributed significantly, demonstrating that even low energy devices in the range of kJ can generate neutrons [15]. However, there are uncertainties regarding the physical mechanisms

involved in the formation of plasmoid. When the breakdown of ionized gas occurs at the insulator sleeve, the plasma sheath undergoes three phases: breakdown, acceleration and radial compression phase.

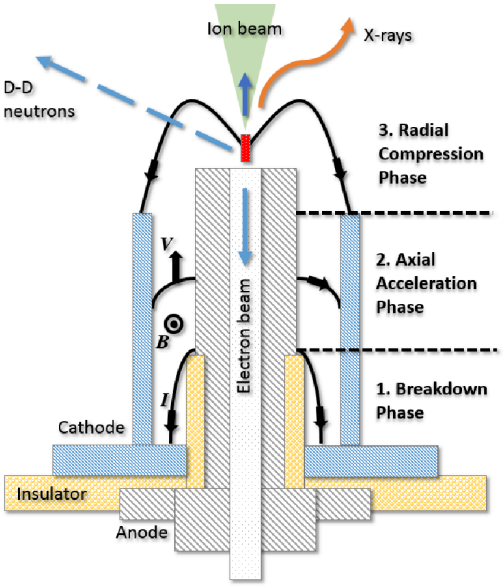

Figure 1.2: Dynamics of the plasma sheath formed in the DPF described as three phases: Breakdown, Acceleration, Radial Compression [2]

1.2.1 Breakdown Phase

When high voltage pulse is applied on the inner electrode of the DPF, a breakdown of gas occurs when it is filled with working gas of suitable pressure. The breakdown begins at the inner electrode after a time delay that causes sliding discharge along the insulator. The sliding discharge reaches the end of the insulator and creates filaments. This filamentary pattern moves toward the outer electrode, with current flowing from the positive electrode along the insulator and towards the outer electrode. This creates a current loop, inducing a magnetic field that produces a force that pushes the plasma sheath radially outwards. The formation of the filaments has been researched extensively. Experiments have shown that

parameters such as anode geometry, insulator length and coaxial gap between electrodes can affect the structure of the filaments [16] [17]. Initial fill pressure also has an important role in the breakdown dynamics and formation of filaments. For any dimensions of electrodes and insulator there is an optimal pressure for uniform plasma sheath. Low pressure can create unsymmetrical discharge sheaths and high pressure can create filamentary structures [11].

1.2.2 Acceleration Phase

After the current sheath is formed at the end of breakdown phase, the $J \times B$ force accelerates the plasma sheath towards the end of the electrode. This force has both radial and axial components. The radial force is outward and the axial force is backward between the inner and outer electrode that causes canting of the sheath as shown in Figure 1.2. The axial force $(J_z \times B_\theta)z$ where B_θ varies $1/r$ which results in higher velocity at the inner electrode [18]. The radial force is much stronger at the outer electrode which leads to less acceleration at the boundary of the outer electrodes. This results in the nonlinear mass buildup along the radial position, where the sheath mass increases linearly with position on the inner electrode but the mass buildup is non existent on the outer electrode which leads to further canting of the plasma sheath. The plasma sheath acceleration is predicted by the snowplow velocity model, developed by Rosenbluth and Garwin [19]. This model is used to calculate the time of arrival of the plasma sheath at the end of the electrodes. [20],

$$V_s = (\frac{c^2 E^2}{4\pi\rho_0})^{1/4} \text{cm/sec} \tag{1.1}$$

Where E is electric field between electrodes, ρ_0 is density of gas and c is speed of light. This velocity relationship 1.1 shows the dependence of driving current on the formation of the plasma focus. The time of arrival of sheath is useful in deciding the DPF parameters such as

optimal gas filling pressure, voltage, center electrode length and the driving current needed.

1.2.3 Radial Compression Phase

At the end of the axial phase the plasma sheath collapses due to the axial and radial forces and converges inwards the center electrode, giving rise to the "pinch" effect. It is known experimentally [21] that most gas escapes during this phase. This effect produces plasma densities of almost 10^{20} cm-3, X-rays near 500 keV, and neutron pulses of the range 10^{12} neutrons per pulse [21] for MJ devices. This phase is important because of the high density of plasma and emission of radiation when operated in deuterium. During the compression, the plasma forms a column and is compressed adiabatically which after some time begins to stagnate [22]. Experiments have shown that the pinch lifetime lasts for a few nanoseconds [23] because the plasma column begins to be hydrodynamically unstable to sausage ($m = 0$) and kink ($m = 1$) instabilities, where m refers to the azimuthal mode number. The growth of $m = 0$ instabilities enhances the induced axial electric field and causes the electrons to move inwards towards the center anode, and the ions in opposite direction. The Pease–Braginskii current is the value of current at which the bremsstrahlung (radiation released by interaction of charged particles) equals the Joule heating of the plasma pinch column in hydrogen assuming Spitzer resistivity [24]. Due to the bombardment of the electrons on the anode, impurities are generated in the plasma column. The impurities decreases the Pease – Braginskii current and causes the plasma column to implode and the disruption continues till the plasma column breaks completely. Due to the breaking of the plasma column, a large and hot plasma cloud is formed which gives rise to bremsstrahlung radiation. Depending on the dimensions of the inner electrode, the diameter of the plasma column is in the order of 1 mm. The neutron pulse reaches its peak value during this phase, and soft X-ray emissions are produced abruptly. It also gives rise to energetic electrons and ions.

1.3 Instabilities

Plasma instabilities pose a significant challenge to the development of controlled thermonuclear fusion. These instabilities limit the amount of current and pressure that can be confined by a magnetic field. In DPF, the magneto-hydrodynamic instabilities grow during the radial collapse phase. Figure 1.3 shows the two MHD instabilties forming in the dense plasma. The $m = 0$ (sausage) instability occurs when the poloidally symmetric radial perturbation constricts the plasma column. This perturbation causes an increase in current density flowing through the narrower radius of the plasma column, resulting in intensified magnetic fields in that region while the remainder of the plasma column remains relatively unaffected. Consequently, these enhanced magnetic fields exert additional inward force, amplifying the constriction in that particular area. The rapid changes in magnetic fields induced by this instability generate significant longitudinal electric fields within the plasma, accelerating ions to energies reaching hundreds of keV. Collision of these energetic ions with lower energy ions leads to the emission of bursts of neutrons. Adding a longitudinal magnetic field stabilizes the sausage instability. There is also formation of kink instability ($m = 1$) that transforms the plasma into helical shape. When the plasma column bends, the poloidal magnetic fields along the inner edge of this bend become stronger than those along the outer edge, intensifying the bending of the plasma column even further. This mode can be stabilized by strong longitudinal field that can create enough tension in the plasma column to prevent bending.

1.4 Neutron Production in DPF

Initially the DPF was researched for thermonuclear fusion because it produced several MeV neutrons [13]. Later it was found that the neutron production is not because of the hot

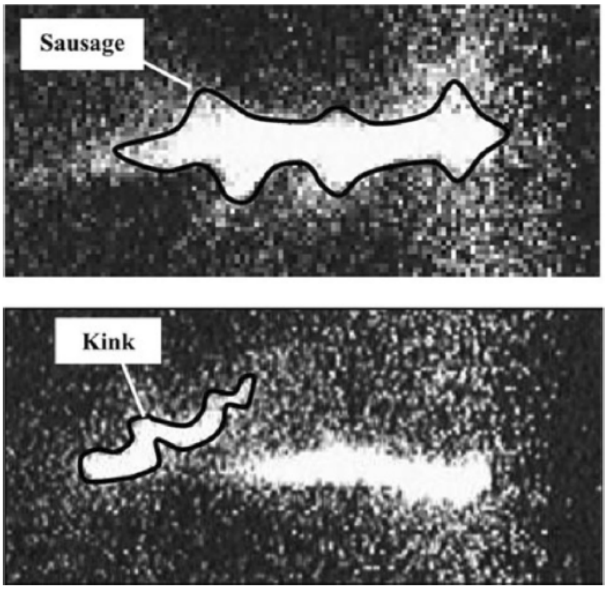

Figure 1.3: Sausage and kink instability captured using X-ray pinhole camera [3]

plasma but involves a non thermal process. When the ions are accelerated during the pinch formation, they interact with the background plasma and produce neutrons through the beam target mechanism. It is found by numerical and experimental investigations that the MHD instabilities intensified the electric fields and increased the axial acceleration of the ions and by suppressing the instabilities the neutron production would lower [25]. The beam target fusion has certain limitations as the fusion cross sections are several orders of magnitude smaller than scattering cross sections. The beam ions have high kinetic energy and are accelerated at high velocities. The accelerated ions collide with other particles and lose energy and scatter reducing the probability of fusion reaction. However, thermonuclear reactions also occur in the plasma and if the ions are confined at higher temperatures it could sustain more fusion reactions.

Many experiments have shown that the DPF neutron production can be increased by optimising the geometry (anode, cathode, insulator) or by changing the paramters such as operating pressure, charge voltage, peak current. It is found that the final pinch compres-

sion lasts a few nanoseconds [23]. It is important that the length of anode has to match the current risetime of the capacitor in order for the compression phase to achieve best efficiency. Two main design parameters of the DPF are the drive parameter and energy density parameter. The drive parameter shows that the axial and radial characteristic speeds of the current sheath depend on $I_0/ap^{1/2}$ where I_0 is the pinch current, a is the anode length and p is the gas filling pressure. Past experiments have shown that for a neutron optimized devices this value is in the range of 89 ± 8 kA/cm with standard deviation of 10% [26]. Energy density parameter 28 E/a^3 was introduced as a tool to determine the anode length [27].

Although the neutron yield was experimentally observed to increase with energy, it was found that it reaches a saturation and starts decreasing with increasing energy [28]. Some studies also found that the inductance of the system has a role in determining the peak current and has a limitation that after reducing the inductance to a certain value it neither increases the pinch current nor the neutron production [29].

1.5 Kilojoule range DPF Devices

Over last decades, a number of PF devices have been developed, ranging in size and energy from MJ to kJ. Among these, devices operating in the MJ energy range have demonstrated capability to generate neutron yield ranging from 10^7 to 10^{12} through D-D fusion reaction. Various heavy fuel gases such as neon and argon have also been studied to understand the production of hard and soft X-rays. In late 20th century, research was emphasized on enhancing power, neutron and radiation power, and discharge current. However, in the last decade there has been a shift in the research focus towards reducing power and discharge current while miniaturizing PF devices. This trend has emerged due to diverse applications of such devices in technologies like materials, radiography and medicine, which extend beyond

energy related pursuits. The various devices and their working parameters are shown in Table 1.1. Devices operating within the MJ and kJ energy ranges share several similarities. Parameters such as the drive parameter, energy parameter, and energy per mass parameter maintain consistent values for optimizing neutron production.

Table 1.1: DPF characteristics of existing devices

Device	Energy (kJ)	Peak Current (kA)	Pressure (mbar)	Fuel gas	Ref
PF 360	106-176	1200-2100	1.6-21.3	D-D, D-Ar	[30]
PF 1	200-490	2000 - 2800	9.33-12	D-T	[31]
PF TAMU	460	3000-4000	13.33	D-D	[32]
UNU - ICTP PFF	1.8 - 3.3	170-250	1.3-5.98	He-D	[33]
PF NX2	1.6-3.3	190-510	0.7-20	H, D, He, Ar, Ne	[34]
PF PFIPS	1.5-1.9	200	0.1-1.3	Ar	[35]
PF BARC	2.2	130-180	0.1-20	N2, Ne, H	[36]
PF DPF - 40	16-18	350-380	0.6-8	D, H	[37]
PF ODAK	3	39	6-14	D-D	[38]

Table 1.2: Scaling Laws for kJ range DPF devices

Neutron Yield	$Y_n \sim E_0^{2.0}$, $Y_n \sim I_{pinch}^{4.5}$
Beam ions at exit of pinch	$Y_{ions} \sim 18.2 E_0^{1.23}$, $Y_{ions} \sim I_{pinch}^{3.7}$

Experimental data from past decades were used to create the scaling laws for the DPF for increased neutron yield [26]. For devices in the range of 1 kJ and less can show enhanced stability by the means of resistive effects. Table 1.2 describes the scaling of neutron yield and

beam ions in 1 kJ and sub kJ range. All devices, irrespective of their size, uphold consistent values for ion density, magnetic field strength, plasma sheath velocity, Alfvén speed, and energy per particle. This uniformity enables the feasibility of achieving fusion reactions even in devices working in kJ range. Scalability laws and design parameters above can be used for construction of such devices to optimize the neutron yield by increasing the energy per particle.

Chapter 2

Experimental System

The DPF at Virginia Tech consists of a center hollow anode surrounded by cathodes forming a squirrel cage configuration. The electrodes are fitted into aluminum cylinder and enclosed in Pyrex glass. The insulator sleeve between the electrodes are made of ceramic alumina. The DPF is fastened to an aluminum plate. The radius and length of electrodes were found by the energy density parameter. The length of the anode and surrounding electrodes are equal. For the device to work optimally, the time of arrival of the sheath to the edge of the inner electrode must coincide with the peak current time.

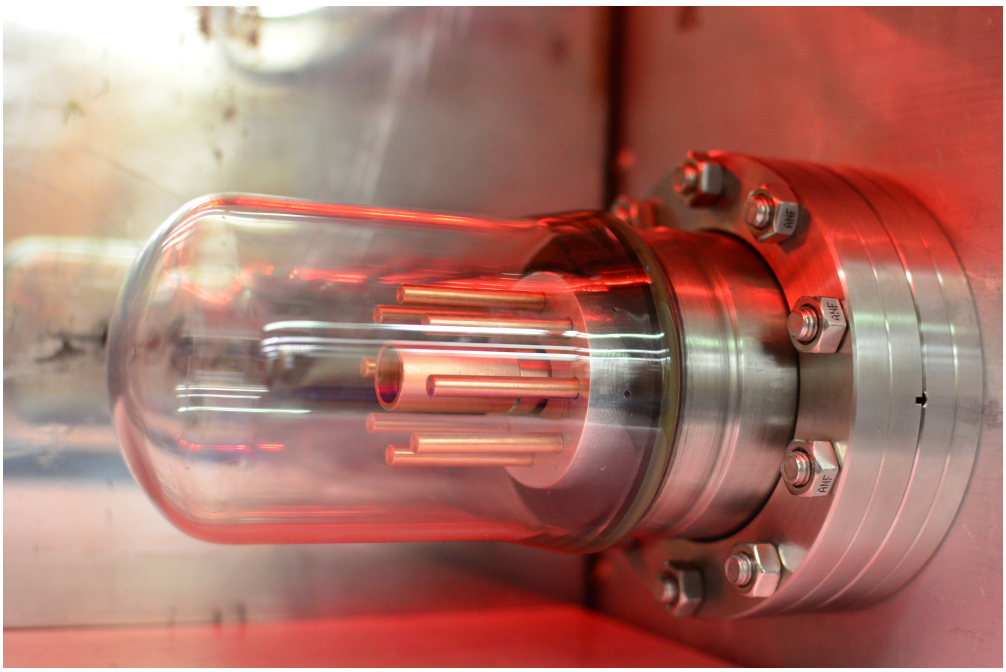

Figure 2.1: DPF device consisting of central anode and cathodes in squirrel cage configuration

A complete DPF system comprises an energy storage and transmission system, a high-energy switch, a vacuum and gas control system, a high-voltage charging system, shielding, grounding, and diagnostics. The system utilizes a capacitor with a capacitance of 1.3 μF, possessing an energy capacity of 1 kJ at 40 kV. For high-voltage triggering, the newly selected spark gap, SG181-C, has been chosen. Given an estimated peak current of approximately 90 kA and a maximum operating voltage of 40 kV, the spark gap is well suited for operation within these parameters. To integrate the new spark gap, modifications were made on the transmission lines and control system that is described in the next section.

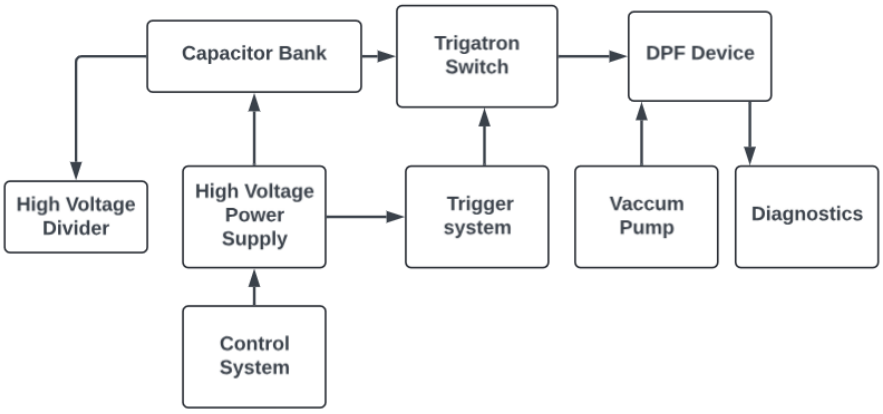

Figure 2.2: Experimental system components of DPF

2.1 Transmission Lines

The SG181-C spark gap is dielectric and measures 10.5 inches in diameter and 3.44 inches in height. To integrate the new spark gap into the experiment, adjustments were required for the bus work connecting the capacitor to the DPF anode. This bus work is constructed from aluminum and designed to minimize inductance. Figure 2.3 shows the new bus work arrangement. It consists of circular top plate and L - shaped alumnium plates connected to

the anode of the DPF. The cylinders connecting the capacitor to the spark gap underwent alteration due to differences in bolt geometry of the spark gap. The cylinder was extended to 4.5 inches to maintain a safe distance between the dielectric sheet at the rear of the capacitor reducing the risk of arcing and the disk diameter is 5 inches. Flat screwheads were selected for fastening the bus work to ensure proper compression of the plates during high-voltage operation. The inductance of the modified bus work is detailed in table 2.1. The total inductance compared with the previous bus work is much higher.

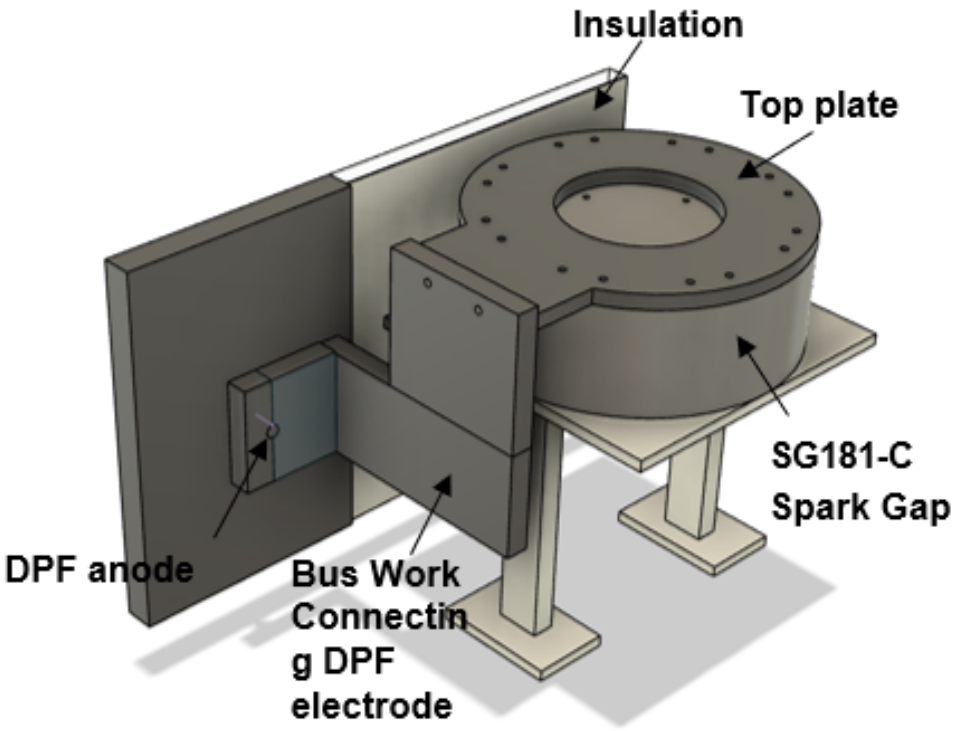

Figure 2.3: CAD model of the bus work connecting Spark Gap to the Electrode of DPF

Table 2.1: Total inductance of the modified bus work compared with the previous bus work

Part	Previous Bus Inductance nH	Modified Bus Inductance nH
Cylinder and disk	45.25	62.64
Plates	45.54	230.76
Spark Gap	30	30
DPF anode	29.4	29.4
Total	150.19	352.8

2.2 Circuit Modelling

LTSpice was used to estimate the peak current of the DPF. This includes the capacitor, the connections between the capacitor and spark gap, the spark gap, the connections from the spark gap to the DPF, the DPF itself, and the return line to the capacitor bank, all connected in series as shown in Figure 2.4. Figure 2.8 shows that the estimated peak current is approximately 65 kA, slightly below expectations due to the increased inductance of the bus work. Despite efforts to minimize bus work dimensions through various means, it was determined that peak current remained largely unaffected unless the inductance dropped below 100 nH. Given the constraints of geometrically lowering the inductance of the bus work, the current design was thus finalized.

2.3 Control System

The DPF operation requires remote operation due to safety considerations, including the arc flash boundary extending 8 feet. The control elements include the charge and dump relay, surge and purge mechanisms of the spark gap, interlocks, and monitoring systems for voltage input, as well as voltage and current from the HV power supply. Modifications were made for remote control, and all the switches are controlled by NI DAQ and operated by

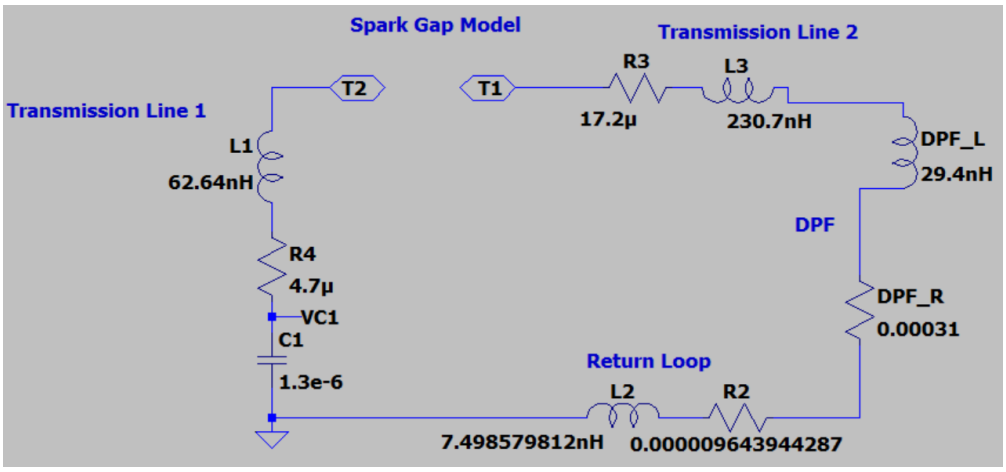

Figure 2.4: LTSpice Circuit of the modified DPF with the new transmission lines inductance and resistances.

LabVIEW. The block diagram describes all the connections of DAQ with DPF controls. The DAQ is connected to two circuit boxes that connects the hardware with coaxial cables and connects to the computer with labview outside the experiment room by a 30 feet long USB cable.

The initial electrical path in the high voltage connection starts from the HV power supply, leading to a diode and resistor setup designed to protect against voltage spikes and reverse voltage. This path then links to the first Ross Relay, which remains neutrally open. In case of emergencies or loss of power it will disconnect the charging of the system and allow the power to go to ground. Another important path of voltage is from the neutrally close relay. It connects to the bottom pf the spark gap which is positive to resistors and finally to the ground. In the scenario of power loss this relay will de - energize the system. The resistor used in this circuit is 100 $k\Omega$ with a dissipation capacity of 16 kJ. The RC time constant of the circuit is 0.13 s, indicating a rapid discharge capability. The last circuit connects the positive bus to the capacitor ground. Two resistors 100 MΩ and 100 kΩ are connected in series which divides the voltage by a factor of 1/1000. It is connected to analog meter to show the charge of circuit. It also acts as a discharge circuit when the dump circuit fails and

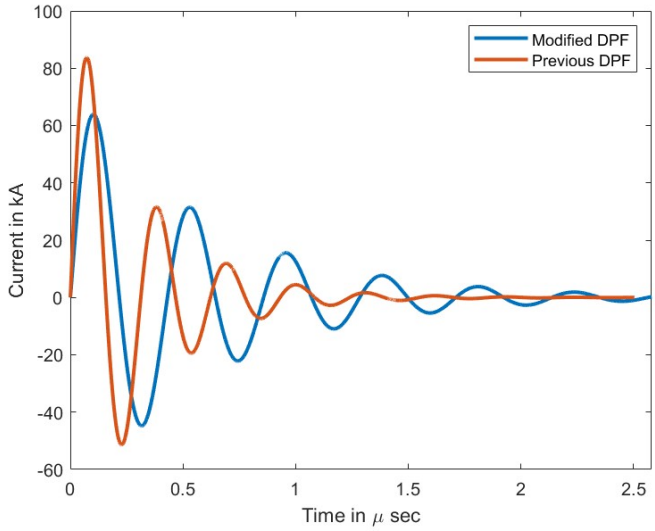

Figure 2.5: Pulse generated in LTSpice shows the predicted peak current difference between the modified and previous DPF.

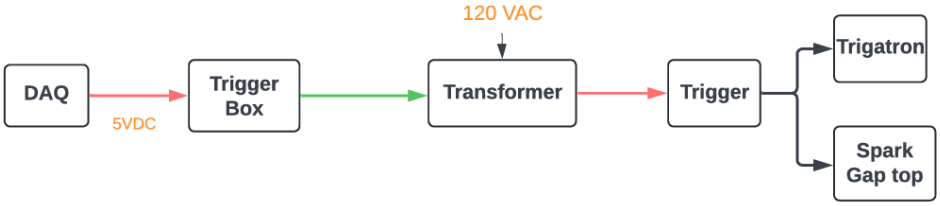

Figure 2.6: Connections of the DAQ to DPF hardware for Trigger control. Green lines are fiber optic cable, Red are coxial cable, Black are HV Rated Wire.

has RC time constant of 130 s. If in any scenario the discharge circuits fail to work, the last safety measure is to use a discharge stick that has a tip connected to a high power resistor.

The circuit used to control the charge and dump relays are described in figure 2.10. The relays are connected to the UPS, to prevent the high voltage from flowing to the main wall ground. A 5 V signal is generated by the DAQ, that sends the signal through a coaxial cable to the circuit. It turns on the AND gate within the transmitter circuit which engages a single pole single throw relay. The transmitted signal is then relayed via fiber optics to the receiver circuit. Upon reception, the 5 V output from the receiver circuit triggers another relay This

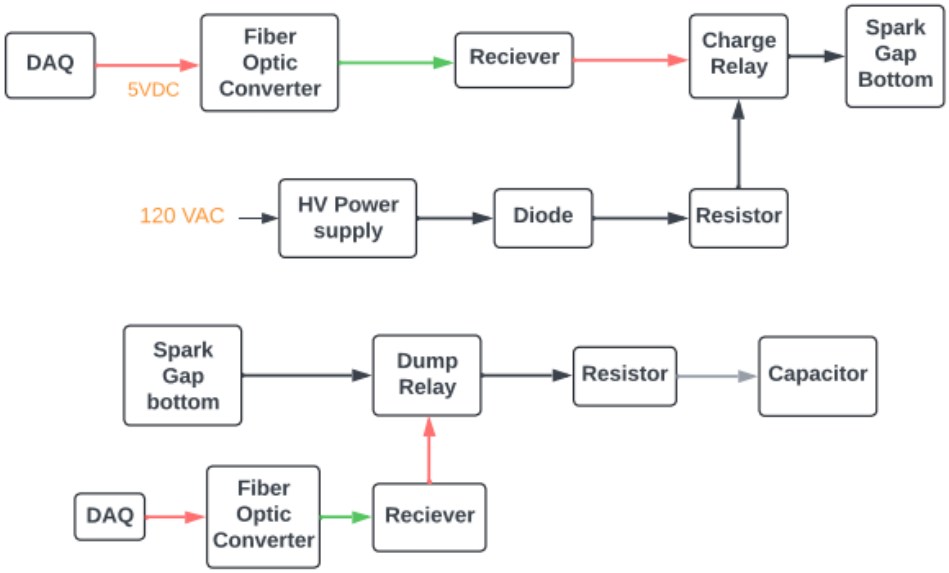

Figure 2.7: Connections of DAQ woth DPF for charge/dump control of relays. Green lines are fiber optic cables, Red are Coaxial cables, Black are HV Rated Wire, Grey are ground wire.

Figure 2.8: Bleed resistor connections for voltage monitoring

relay is connected to a 120VAC converter and the output is connected to the neutral of three pin socket that will activate the charge/dump relays.

In case of an emergency, there is a red button integrated into the relay hardware. This button functions as a normally closed switch and is operated externally to the experiment room. Both the interlocks and the red button are linked to a double pole single throw (DPST) relay switch as shown in figure. When the interlocks are turned on the HV supply, and the emergency button remains disengaged, a 5V signal is sent to the relay via the fiber optic circuit. However, if either the emergency button is pressed during an emergency or the

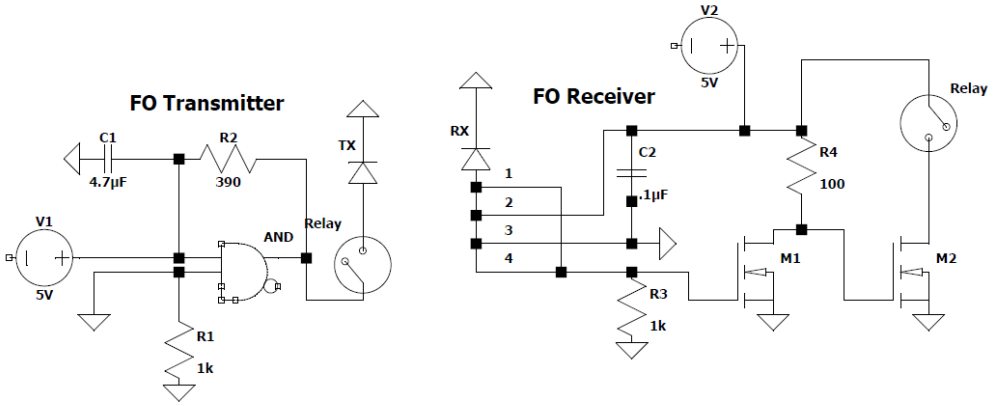

Figure 2.9: Fiber optic circuit

interlocks are inactive, the charge/dump control will not be engaged.

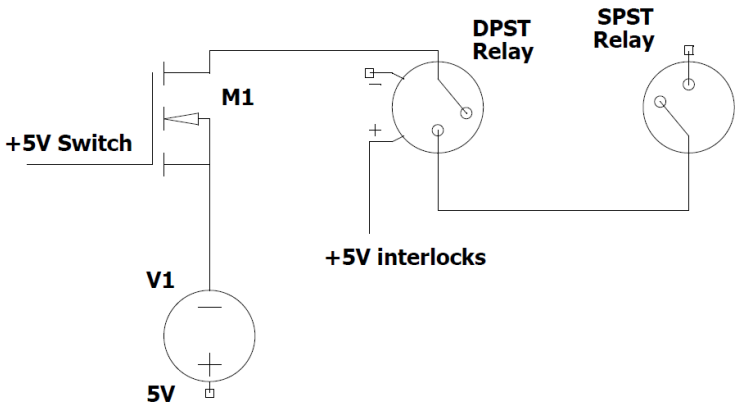

Figure 2.10: DPST Relay connected with red button and interlocks

Controls on LabVIEW include the on/off swicthes for relays, interlocks, HV enable, purge/-surge of the valves and trigger. In addition to integrating the red button with hardware, it is also integrated into the LabVIEW with relay buttons and the HV power supply interlocks by an event structure. Detailed LabVIEW structure can be found in Appendix B. The event structure has two event cases out of which one executes when the event is identified. It has a timeout of 20 milliseconds to wait for an event to occur. The first event is when the red button is not engaged, it sends a 5V signal to the DAQ input which is read by the event

structure as a boolean. As it is identified as true, the event structure then allows to 'write' on either of the charge/dump relays. When the red button is engaged, the boolean will be false and the structure will return the relays to their normal state. In the same way the interlocks are also depended on the emergency button on the LabVIEW. The other controls of the HV supply are the current and voltage monitor. The DAQ is connected to the HV supply pins by a coaxial cables. For voltage monitor the power supply sends a 1- 10 VDC signal which is directly proportional to 0 - 150 kV. All of the on/off switches on control panel are while loops that will run until it is terminated with the stop button.

Chapter 3

Numerical Modelling

To understand the dynamics of plasma sheath, theoretical models have been developed over the last decades. One of the models proposed was a magneto-hydrodynamic model, coded by Sing Lee in 1984. This code was used to show the dynamics of the early stages of the plasma and was later modified to also incorporate the complete image of phenomena occurring in the radial phase. The code uses the electrical electric circuit of the device and combines it with the plasma focus dynamics to show near realistic image of the pinch formation properties. It allows in predicting the design of PF, temperature, density and emission of radiation. The scope of this model is described in Figure 3.1. The dynamics is divided into five phases - axial phase, radial inward shock phase, radial reflected shock phase, slow compression phase, and extended column phase.

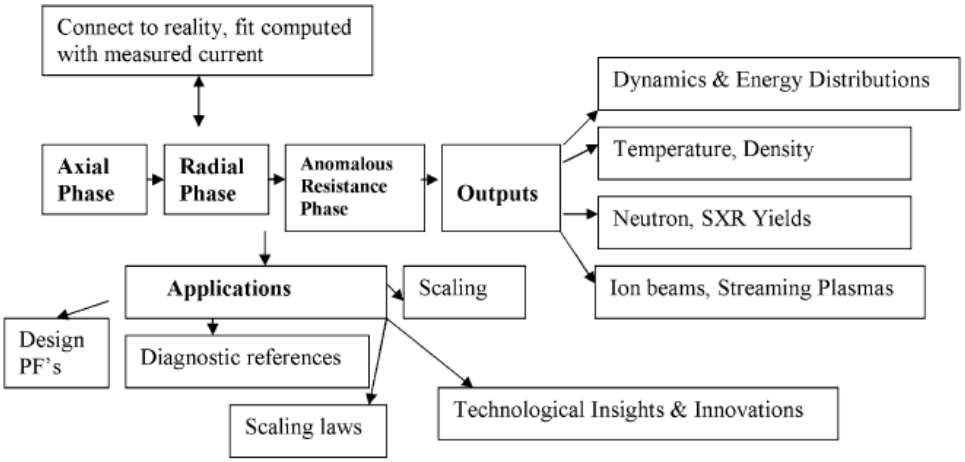

Figure 3.1: Schematic of the lee model showing the philosophy and application

3.1 Five phases of the Lee model

The Lee model describes the plasma dyanmics of the DPF by five phases: axial, radial inward shock, radial reflected shock, and slow compression phase. Snowplow model is used to describe the axial phase where the equation of motion is coupled with the circuit equation. The parameters incorporated in these equations are the f_m (mass swept up factor) and f_c (current factor). For modelling purposes the plasma layer is a conductive sheath that sweeps from the anode bottom to the top. To account for the effects on amount of mass in the moving structure, the mass swept up factor f_m is used. f_c is defined as the fraction of current effectively flowing through the current sheath. The main purpose of these parameters is to delay the pinch formation until the current reaches the peak.

The radial inward shock phase integrates four equations that are the radial inward shock speed, the axial elongation speed, the speed of the current sheath and circuit equation using a slug model. A detailed description of these equations are given in [39]. A slug model is used to couple the four equations describing the phenomenon of radial inward shock. A reflected shock moves radially outwards when the shock front hits the axis and simultaneously causes the annular column to elongate. This phase begins with the position of magnetic piston and the shock front being equal. Temperatures and number density are computed during this phase. The radial phase mass swept-up f_{mr} and the current factor f_{cr} are incorporated in all the three radial phases. The f_{mr} accounts for the mechanisms that affect in reducing or increasing the amount of mass in the moving slug and the f_{cr} accounts for fraction of current effectively driving the radial slug.

When the reflected shock collides with the magnetic piston, the compression phase starts and increases the temperature and density of the pinch. A reflected shock is developed which moves radially outward while the magnetic piston moves radially inward and the phase ends

when the reflected shock and the magnetic piston compresses the pinch to a certain radius. The model parameters f_{mr} and f_{cr} are also used as in this phase.

After the reflective shock phase, slow compression phase starts. It is also called as the radiation phase since only for this part the pinch is emitting x rays. Radiation yields and thermonuclear beam target components of neutron yields are computed in this phase.

In the last phase, snowplow model is used to simulate the current trace after the pinch. The radial reflected shock phase and the pinch phase occurs in a very short time as observed in laboratory measurements due to the plasma current disruptions.

The neutron yield is calculated using two components: thermonuclear and beam target. The thermonuclear component is described as:

$$\mathrm{d}Y_{\mathrm{th}} = 0.5 n_i^2 \pi r_p^2 z_f \langle \sigma v \rangle \tag{3.1}$$

The thermonuclear term is obtained by summing up over all the intervals of focus pinch. The beam target component is defined as:

$$Y_{b-t} = C_n n_i I_{\mathrm{pinch}}^2 Z_p^2 \left(\ln \frac{b}{r_p} \right) \frac{\sigma}{V_{\mathrm{max}}^{1/2}} \tag{3.2}$$

The beam target term is found to be far more dominant than the thermonuclear term. This yield is proportional to the beam ion speed v_b and this speed is $\sim U$, the beam energy. The term U is fitted to be 3 times the V_{max} to align with the experimental observations.

3.2 PLADEMA model

A theoretical model PLADEMA was developed by researchers associated with the Inter-institutional Program of Dense Magnetized Plasmas, National Research Network [40] to explain the neutron production and its relation to filling pressure, current and geometrical parameters. This model uses the snowplow model for the acceleration phase and assumes that the neutron emission is mainly through thermonuclear reactions. The plasma is assumed to follow the Bennett equilibrium [41], meaning that the plasma is in radial pressure balance with the magnetic field. This relation is used to define the temperature at the pinch phase. The model is benchmarked against small PF devices and variation of filling pressure and anode length [42]. The thermonuclear neutron yield is defined as:

$$2Nk(T_e + T_i) = \frac{\mu_0}{4\pi} I^2 \tag{3.3}$$

Where N is the number of electrons per unit length, T_e is the electron temperature, T_i is the ion temperature, I is the beam current

$$\frac{Y}{h} = \frac{1}{128}\left(\frac{\mu_0}{4\pi}\right)^2 \sqrt{\frac{3m_i\langle\sigma v\rangle Z^2}{(kT^*)^5}} \frac{I^4}{r_S} \theta_B^{-\frac{29}{12}} \exp\left(-\theta_B^{-\frac{1}{3}}\right) \tag{3.4}$$

Where m_i is deutron mass, $\langle\sigma v\rangle$ is thermonuclear cross section, T^* is cross section parameter in Kelvin. Here θ_B is the dimensionaless temperature related to the Bennett radius (radius of plasma column in bennett equilibrium) using isentropic hypothesis $r_B = r_S\theta_B^{-\frac{3}{4}}$, where r_B is the Bennett radius.

The pinch current is determined in the axial phase. It is defined by assuming a 1-D current sheet integrated with the electrical circuit. The pinch current is defined as

$$I = Q_0 \omega \sin \omega t \tag{3.5}$$

Where Q_0 is initial charge of capacitor. The current varies with operating pressure p_0 with the relations:

$$x^2 = \frac{lQ_o^2}{4m}(t^2\omega^2 - \sin^2 \omega t) \tag{3.6}$$

$$m = \frac{\pi \left(r_2^2 - r_1^2\right) \xi_A m_i p_o}{kT_o}. \tag{3.7}$$

Here x is the axial coordinate, m is the collected mass in unit length.

Both models utilize the snowplow hypothesis can be understood as the process of transferring energy from the capacitor bank to a dense, magnetized plasma structure to describe the motion of the current sheath. The Lee model offers detailed insights into plasma dynamics, using the slug model to calculate plasma thickness during the radial phase. It relies on experimental values, such as gas pressure and static inductance from the current waveform (though these can be adjusted to correct errors). In contrast, the PLADEMA model treats these parameters as variables that can be tuned to optimize the device. The PLADEMA model also introduces the parameter ξ_a (axial sweep efficiency) to account for shape effects. While the Lee model is useful for understanding plasma dynamics, the PLADEMA model is ideal for optimizing the device for thermonuclear yields.

Chapter 4

Results and Discussion

4.1 Current Waveform

The current waveform from the LTSpice for the modified DPF showed the peak value at 65 kA. For Lee model code, the current waveform from experiment has to be fitted using the fitting parameters for accurate predictions. For this the experimental waveform from previous DPF is used as reference. Since the waveform has the peak at 72 kA, it is scaled down to 65 kA. Figure 4.1 shows the experimental waveform and figure 4.2 shows the Lee model fitting. The final parameters of the fitting parameters are $f_m = 0.07$, $f_c = 1.35$, $f_{cr} = 1.1$ and $f_{mr} = 0.8$.

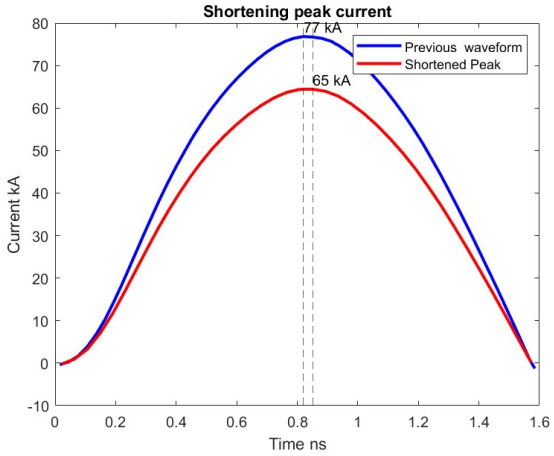

Figure 4.1: Previous experimental waveform of 77 kA scaled down to match the predicted peak current of 65 kA of the modified DPF.

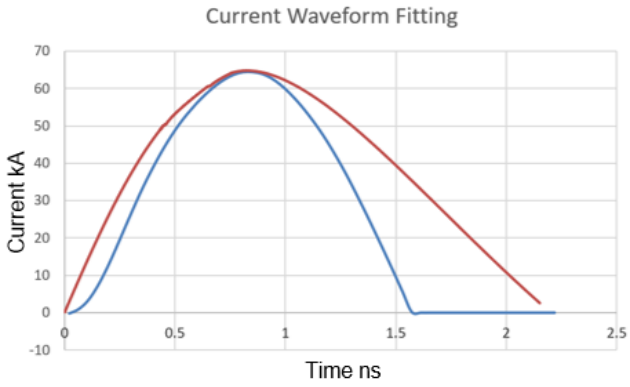

Figure 4.2: Fitting of the current waveform in in the Lee model (red) to the scaled waveform (blue)

4.2 Radial Trajectories

As the pressure is increased, the radiative cooling should affect the pinch radius. Figure 4.3 shows the radial trajectories at various pressures. Figure 4.3a is a reference figure of radial trajectory at 0.5 torr. The radial shock wave starts at 4.79 mm and travels to the axis in 19.6 ns. The reflected shock then hits the magnetic piston at 25.7 ns. At this moment the pinch compresses the column into a pinch of radius 0.742 mm. The temperature at this pinch is 1.6 eV. After increasing the pressure to 2 torr the pinch radius increases to 0.744 mm. At 4 torr the pinch radius reaches 0.749 mm with temperature of 0.3 keV and the pinch starts much later after 40 nanoseconds. At 5 and 6 torr the radius increases to 0.752 mm. The pinch start time is seen to be increasing with the increase in gas pressure. The length of the pinch is maximum at 3 torr, reaching 9.19 cm. The radius of the pinch at this phase depends on the pinch current and the time it takes to reach the peak current. If the timing of the plasma sheath collapsing matches with the peak current time, it results in formation of more neutrons.

Figure 4.4 shows the peak current values at different pressures. The peak current increases

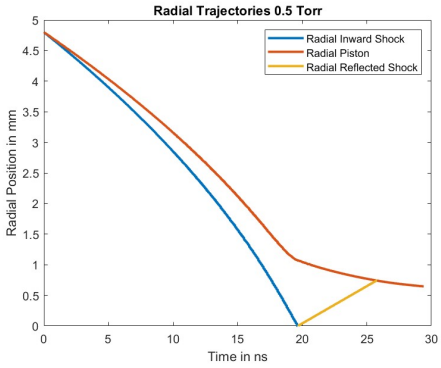

(a) 0.5 Torr

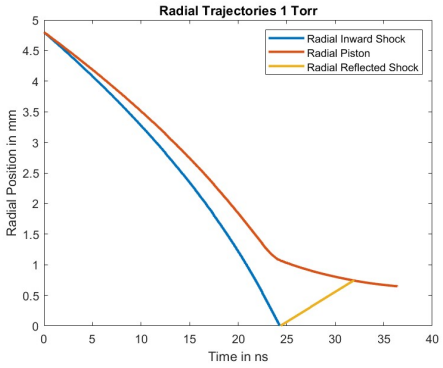

(b) 1 Torr

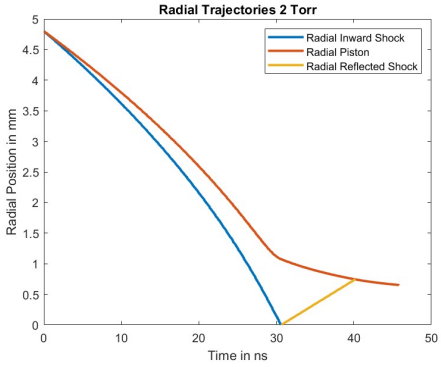

(c) 2 Torr

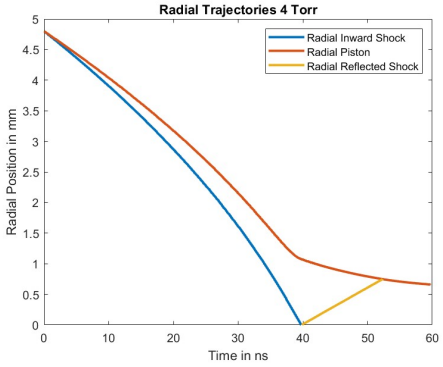

(d) 4 Torr

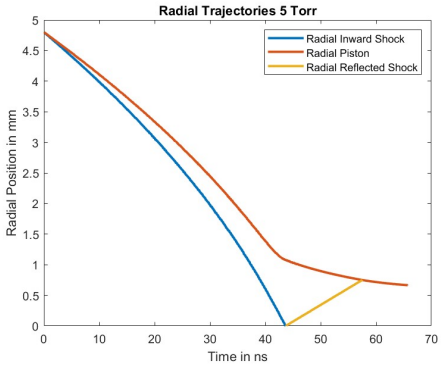

(e) 5 Torr

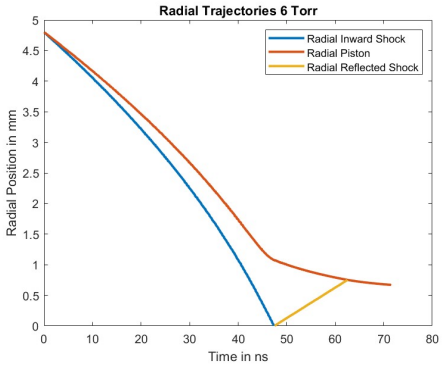

(f) 6 Torr

Figure 4.3: Radial Trajectories at 0.5, 1, 2, 3, 4, 5, 6 Torr. Time in ns from radial start of phase. The radial start time and radius of the pinch increases with pressure.

at 0.5 torr at 50 kA to 71 kA at 7 torr. It shows that the peak current increases with increase in pressure and is an ideal range for neutron production. This increase is due to decreased resistance loading on the plasma sheath which slows down during the radial phase. The peak current decreases after 7 torr which is due to the sheath not collapsing at the current risetime. The pinch forms at around 70 ns which is right before the current rise time. The pressure range from 0.5 - 7 torr would be the ideal range for neutron production.

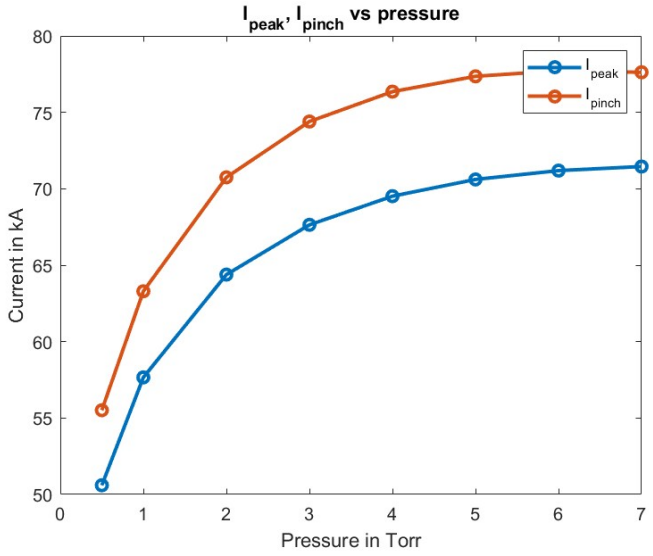

Figure 4.4: Peak and pinch current increases with pressure

4.3 Neutron Production

In this section the neutron yield per shot is predicted at various pressures using the two models: Lee and PLADEMA. The Lee model gives a prediction of total neutron yield and PLADEMA model shows the thermonuclear yield. As seen in Figure 4.5a the total neutron yield for Lee model is maximum at 4 torr. It is to be noted that the thermonuclear yield in the model becomes less significant with increasing pressure. As seen in Figure 4.5b the thermonuclear yield increases from 0.5 torr and is maximum at 2 torr and then decreases

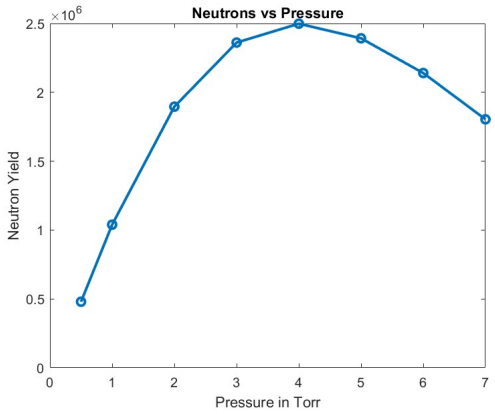

(a) Lee model

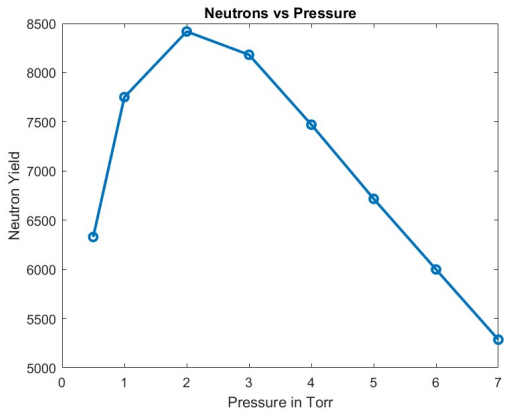

(b) PLADEMA Model

Figure 4.5: Comparing the peak neutron yield in two models: Lee model at 4 torr and PLADEMA model at 2 torr

rapidly. The plasma temperature in this phase is in the sub-keV range as seen in Figure 4.6 and decreases exponentially with the mismatch of pinch current with pinch time.

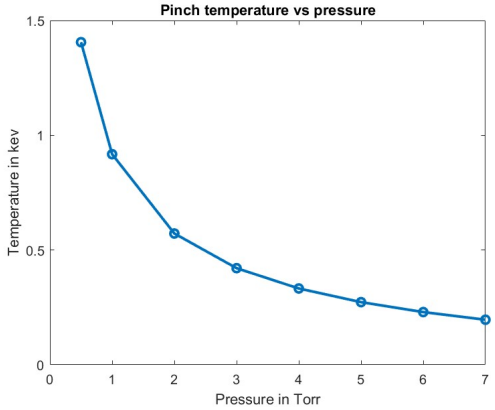

Figure 4.6: Pinch temperature decreases with increasing pressure

Although the neutron yield peaks at 4 torr, the pinch radius is not minimum or the peak current is not maximum as described in 4.2. Figure 4.7 shows the neutron yield comparison with various pinch currents in both the models. It is evident that the maximum yield in both the models occurs when the pinch current is 70 kA. The analytical axial speed of the plasma sheath is described by the speed factor $I/ap^{0.5}$ where I_0 is the pinch current,

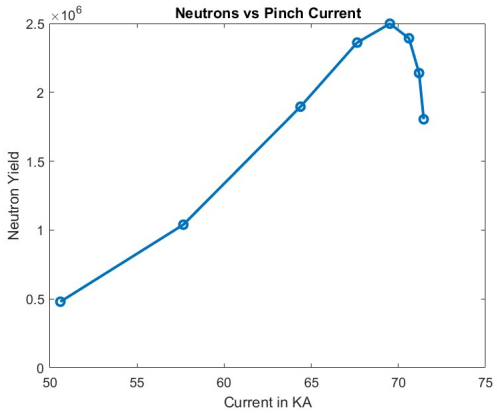

(a) Lee model

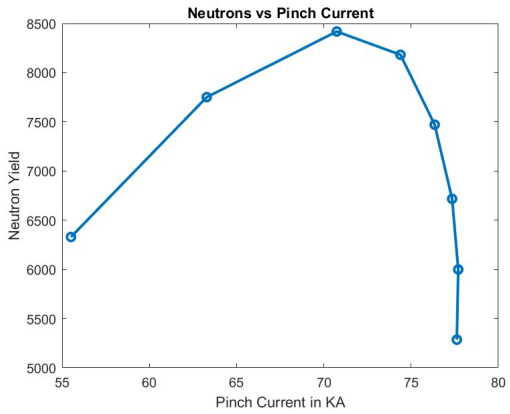

(b) PLADEMA model

Figure 4.7: Comparison of neutron yield and pinch current in two models, showing peaks within the same range

a is the anode length and p is the gas filling pressure. This equation indicates that the velocity of the current sheath in a DPF device with a fixed anode radius and current is proportional to the square root of pressure. However, as the current sheath moves faster, an opposing electromagnetic force (EMF) reduces the voltage, causing the current in the sheath to decrease. Consequently, when pressure increases the sheath velocity decreases due to the corresponding reduction in current. This also affects the temperature, as shown in the Figure 4.6. The yield is also dependent on the pinch duration. The pinch duration is seen to be increasing with increasing pressure. Figure 4.8 shows how the pinch duration varies with the pinch current. Both the models show similar trends and close values for pinch current and duration.

Comparing how the yield varies with the pinch duration as shown in figure 4.9, it is observed that the maximum yield occurs at duration of 5.5 ns in PLADEMA and 6.5 ns in Lee. Although pressure is one of the main variables in determining the neutron production, the peak current and pinch duration also have a significant role.

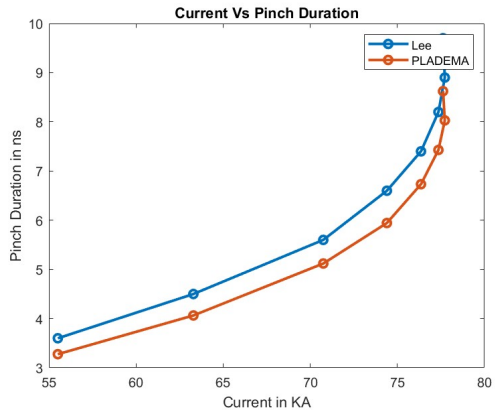

Figure 4.8: Comparison of pinch duration with the pinch current in two models showing similar values

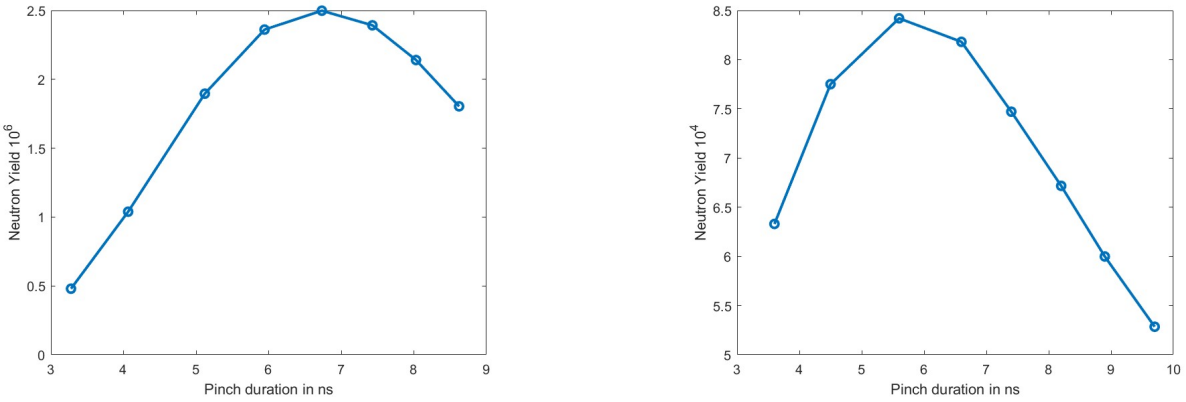

(a) Lee model (b) Pladema Model

Figure 4.9: Comparison of neutron yield in two models showing peaks within the same range

4.3.1 Comparing with previous DPF

The modifications on the DPF had changed the peak current of the circuit from 95 kA to 65 kA. The previous DPF would have different pinch dynamics that would affect the neutron yield. As seen in Figure 4.10, the neutron yield in the modified DPF is higher than the previous DPF.

Although the peak current of the previous device is much higher it yielded less neutrons. This could be due to the energy of the DPF since it was operated at 35 kV with energy of

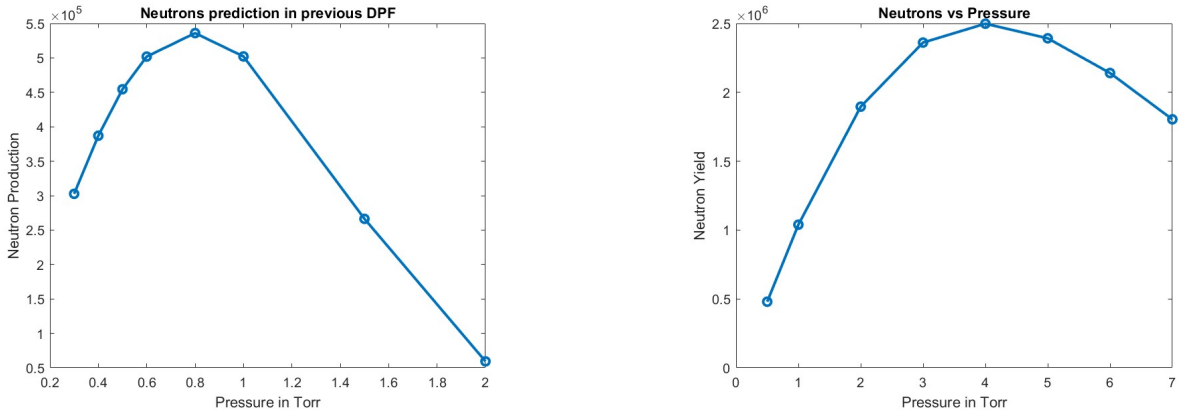

(a) Previous DPF (b) Modified DPF

Figure 4.10: Neutron yields comparison with old and modified DPF

800 J compared to the modified DPF which is operated at 40 kV with energy of 1 kJ. Figure 4.11 shows the scaling of the pinch current with the neutron yield. The scaling is done with the pinch current exponents of 2, 4 and arbitrary value that best fits. Scaling factor that has minimum error shows that the modified DPF scales with pinch current as $Y_n = I_p^{4.7}$ and the previous DPF scales as $Y_n = I_p^{7.5}$.

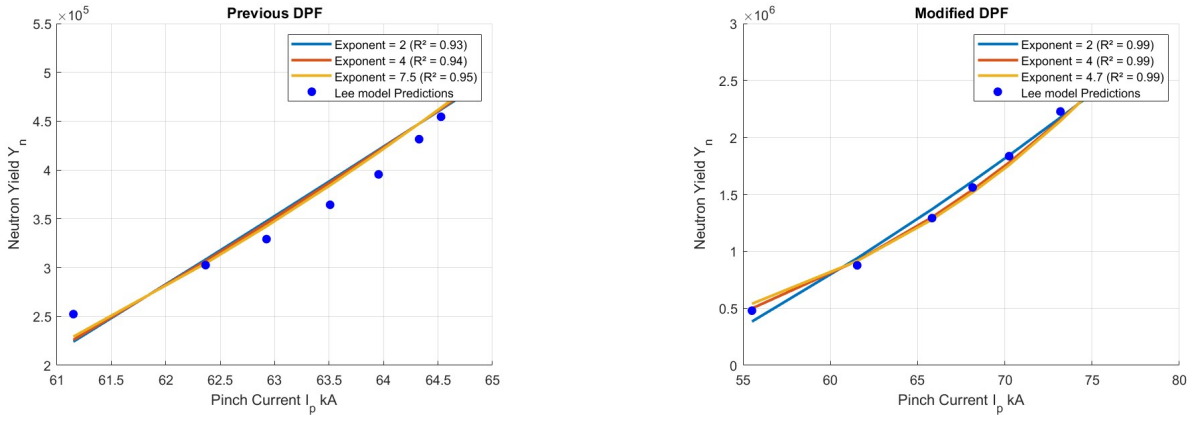

(a) Previous DPF (b) Modified DPF

Figure 4.11: Neutron yield scaling with pinch current for previous and modified DPF

The main difference between the DPFs is the inductance. Although lower inductance show higher peak current as seen in previous DPF, the pinch current formed at the radial start

phase will have a sharp current drop from the pinch phase. Compared to the DPF with higher inductance and lower current waveform, the pinch current will decrease slower and will have a flattened top. This may give more time for the peak current to maintain as the radial compression starts to take place, thus enabling the current rise time to match with pinch formation. Another aspect of the current waveform is the timing of the current dip. If the dip occurs after the peak current, it indicates that the pinch phase is not aligned with the peak. With the charging voltage on the modified DPF increased to 40 kV, the plasma sheath moves faster. However, due to the high inductance of the driving circuit the peak current is shorter. This may have allowed the current dip to happen at the optimal time. To optimize the operating parameters, the pinch time should closely coincide with the peak current. Therefore, if the operating voltage is set at 40 kV, the deuterium gas pressure should be maintained around 4 torr.

Chapter 5

Conclusion

The presented research details the modification on the DPF that includes the bus work to support spark gap, modifications in the pulsed power system circuits for operating the device. These modifications have a significant impact on the current formed which is crucial in determining the neutron yield. Numerical experiments have been performed using two models to compare the predicted neutron yield with the previous DPF. The modifications on the bus work led to changes in the inductance of the DPF circuit. These changes were incorporated in the LTspice model to analyse the current waveform which showed a decrease in the peak current than the previous DPF.

Lee model was used to analyse the radial trajectories of the pinch formation during the radial phase. The pinch radius was predicted for a range of pressures and showed an increasing trend with increasing pressure. Lee model showed that peak neutron yield for beam target fusion is at 4 torr and PLADEMA model showed that the thermonuclear neutron yield peaks at 2 torr. The thermonuclear yield is much lower in order than the beam target model. However, both the models predicted similar pinch current and pinch duration for the highest neutron production. Although the pulse formed in the modified DPF is lower, this might be due to the overall energy of the device that is higher than the previous since it was operated at higher voltage. However, scaling of neutron yield with pinch current in both modified and previous DPF showed that the previous DPF scales much higher. The numerical analysis shows that operating the DPF at optimal pressure can increase the neutron production and

the beam target mechanism mainly depends on the pinch current and duration.

The scaling of neutron yield with pinch current in both the modified and previous DPF revealed that the previous DPF had a significantly higher scaling. The plasma formed in this process acts as a time-varying inductance. A higher inductance in the driver circuit increases the overall inductance of the plasma focus, leading to reduced sheath velocity and a lower plasma temperature. Therefore, for optimal thermal plasma, the system's inductance must remain low, which explains the higher neutron scaling in the previous DPF. The neutron scaling of the modified DPF device has been predicted to follow the fourth power of the current, consistent with previous experiments. Optimizing neutron production requires maximizing energy transfer from the capacitor bank to the pinch phase. To increase thermonuclear yield, lower pressure is necessary to maintain high temperatures, though there is a minimum pressure threshold for gas breakdown. If validated by experiments, analyzing the current waveform from the Lee model offers deeper insights into the mechanisms of neutron production. The waveform can be used to correlate with the voltage spike to determine if in smaller DPF systems the spike occurs simultaneously with the pinch or with a slight delay. Previous studies on higher-energy devices showed neutron production sometimes occurring before the pinch phase. The pinch duration from the two models can be used to see when neutron production happens whether during, before, or after the pinch. This analysis will further illuminate the behavior of smaller, kJ range devices.

5.1 Future Work

The results from the numerical model should be validated by experiments. Current trace from Rogowski coil would give more accurate results from the models. The inductance can be lowered by using different geometry for the bus work. The device can be operated in

different gasses or mixture of gasses to study the effect on neutron yield. Time correlation between dI/dt with the neutron production and X-rays can provide a clearer picture of the neutron emission process involved. In small PF devices, the magnetic energy generated may be insufficient to confine the neutrons. To determine if the neutron production is thermonuclear, measurements can be taken to trace the path of the neutrons and verify whether they remain within the pinch column.

Appendices

Appendix A

Bus Work

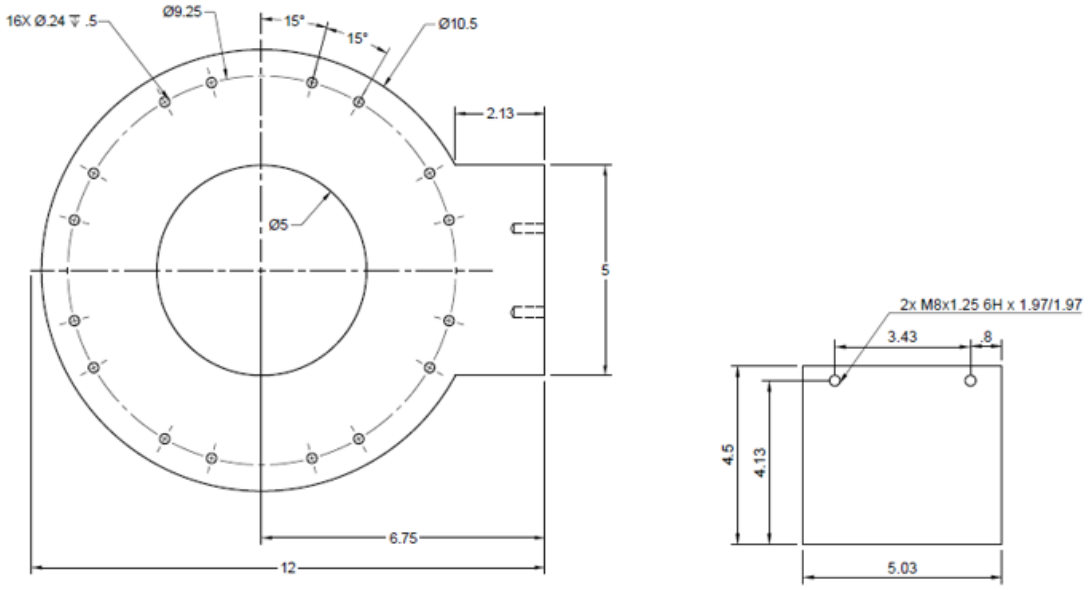

Figure A.1: Top plates connecting spark gap

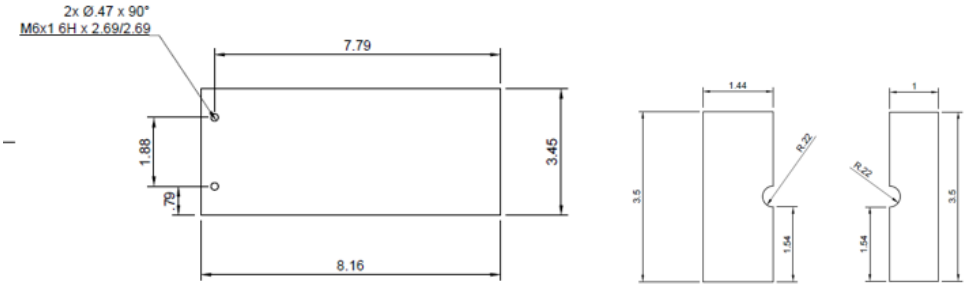

Figure A.2: L - shaped structure blocks

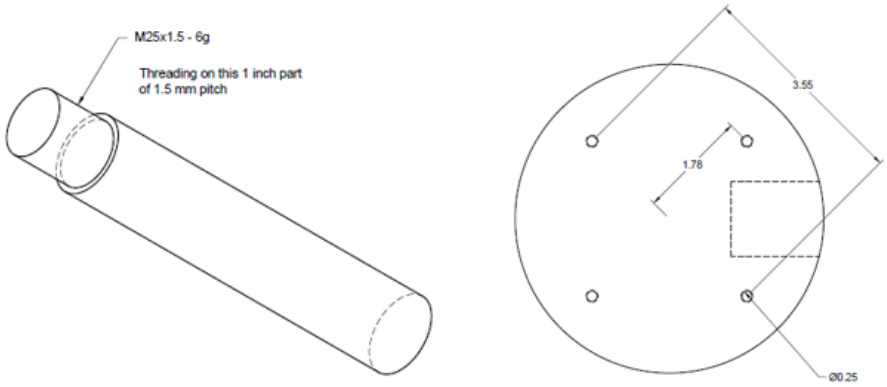

Figure A.3: Cylinder and disk

Appendix B

LabVIEW

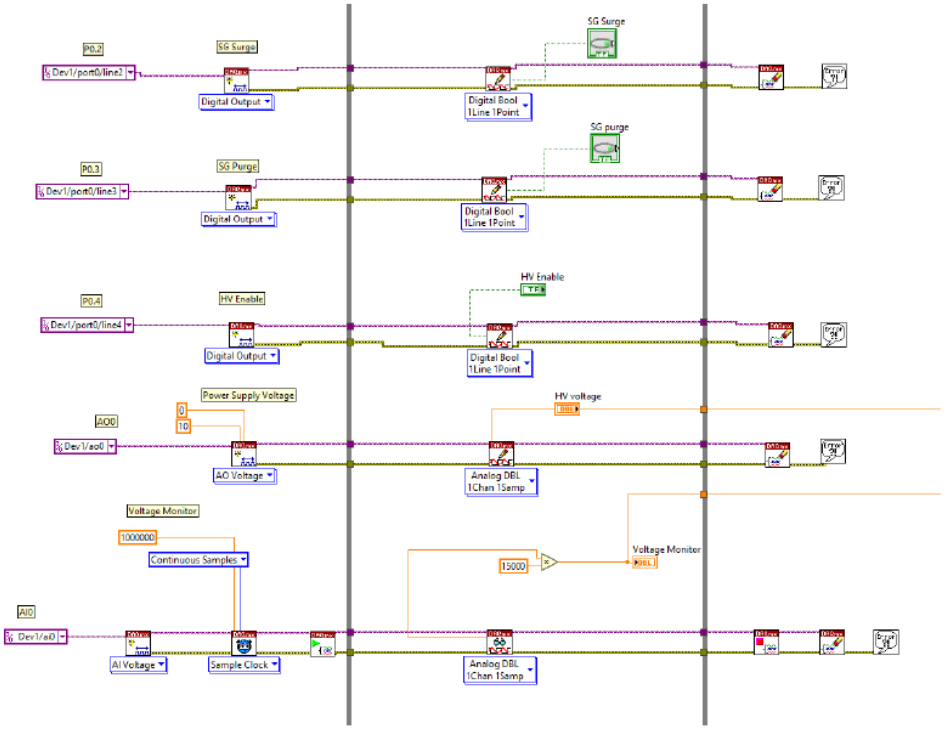

Figure B.1: Loop in LabVIEW for the controls on DPF

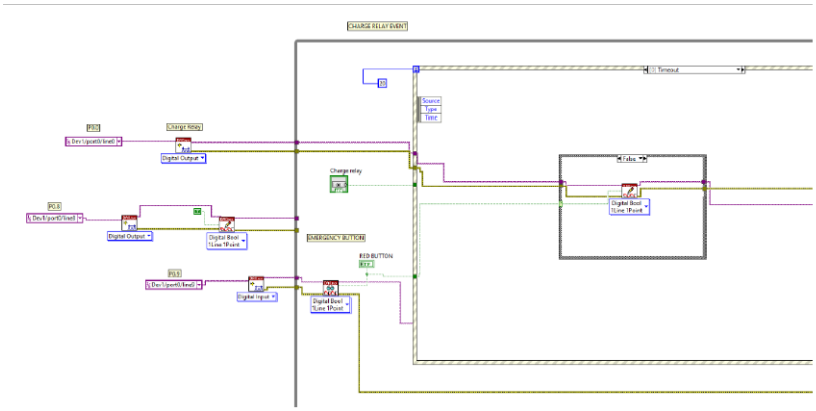

Figure B.2: Event structure for integrating red button with the relay hardware

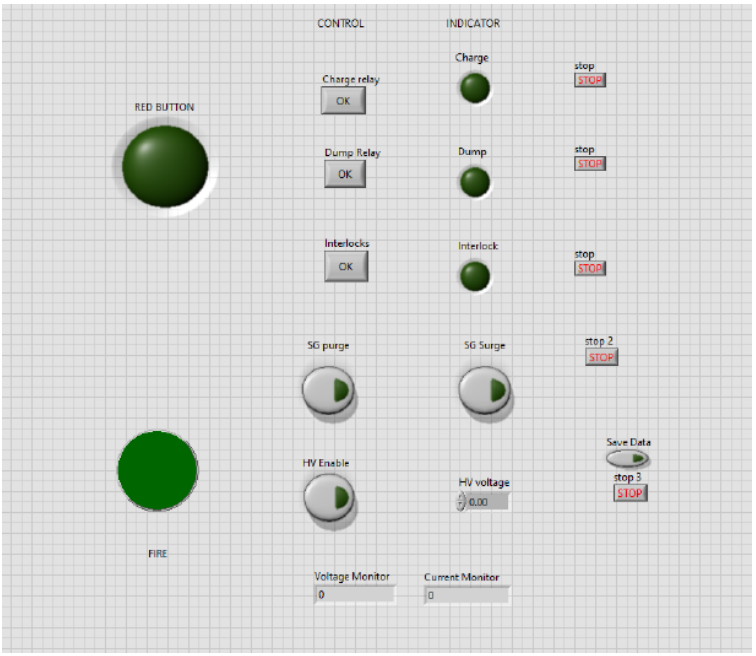

Figure B.3: Control panel

Bibliography

[1] S. Springham, R. Verma, M. Zaw, R. Rawat, P. Lee, A. Talebitaher, and J. Ang, "Plasma focus neutron energy and anisotropy measurements using zirconium–beryllium pair activation detectors," *Nuclear Instruments and Methods in Physics Research Section A: Accelerators, Spectrometers, Detectors and Associated Equipment*, vol. 988, p. 164830, 2021.

[2] S. Chung, "Simulation and characterization of a dense plasma focus device," 2018.

[3] F. E. . S. L. Dubinov, A.E., "Research with plasma foci in countries of asia, africa, and latin america.," *Rev. Mod. Plasma Phys. 4, 6*, 2020.

[4] P. Rebut, R. Bickerton, and B. Keen, "The joint european torus: installation, first results and prospects," *Nuclear Fusion*, vol. 25, p. 1011, sep 1985.

[5] C. I. T. and W. N. R, "An overview of shared technical challenges for magnetic and inertial fusion power plant development," *Phil. Trans. R. Soc. A.37920200019*, 2020.

[6] A. B. Zylstra, A. L. Kritcher, O. A. Hurricane, and et al, "Experimental achievement and signatures of ignition at the national ignition facility," *Phys. Rev. E*, vol. 106, p. 025202, Aug 2022.

[7] U. Shumlak, "Z-pinch fusion," *Journal of Applied Physics*, vol. 127, p. 200901, 05 2020.

[8] W. H. Bennett, "Magnetically self-focussing streams," *Phys. Rev.*, vol. 45, pp. 890–897, Jun 1934.

[9] R. F. Post, "Controlled fusion research—an application of the physics of high temperature plasmas," *Rev. Mod. Phys.*, vol. 28, pp. 338–362, Jul 1956.

[10] J. Mather, "15. dense plasma focus," in *Plasma Physics* (R. H. Lovberg and H. R. Griem, eds.), vol. 9 of *Methods in Experimental Physics*, pp. 187–249, Academic Press, 1971.

[11] J. W. Mather, P. J. Bottoms, J. P. Carpenter, A. H. Williams, and K. D. Ware, "Stability of the Dense Plasma Focus," *The Physics of Fluids*, vol. 12, pp. 2343–2347, 11 1969.

[12] J. W. Mather, "Investigation of the High-Energy Acceleration Mode in the Coaxial Gun," *The Physics of Fluids*, vol. 7, pp. S28–S34, 11 1964.

[13] A. Bernard, P. Cloth, H. Conrads, A. Coudeville, G. Gourlan, A. Jolas, C. Maisonnier, and J. Rager, "The dense plasma focus — a high intensity neutron source," *Nuclear Instruments and Methods*, vol. 145, no. 1, pp. 191–218, 1977.

[14] L. Soto, "New trends and future perspectives on plasma focus research," *Plasma Physics and Controlled Fusion*, vol. 47, p. A361, apr 2005.

[15] L. Soto, C. Pavéz, J. Moreno, L. Altamirano, L. Huerta, M. Barbaglia, A. Clausse, and R. E. Mayer, "Evidence of nuclear fusion neutrons in an extremely small plasma focus device operating at 0.1 Joules," *Physics of Plasmas*, vol. 24, p. 082703, 07 2017.

[16] C. Pavez, M. Zorondo, J. Pedreros, A. Sepúlveda, L. Soto, G. Avaria, J. Moreno, S. Davis, B. Bora, and J. Jain, "New evidence about the nature of plasma filaments in plasma accelerators of type plasma-focus," *Plasma Physics and Controlled Fusion*, vol. 65, p. 015003, nov 2022.

[17] E. N. Hahn, S. Ghosh, V. Eudave, J. Narkis, J. R. Angus, A. J. Link, F. Conti, and F. N. Beg, "Effect of insulator length and fill pressure on filamentation and neutron production in a 4.6 kJ dense plasma focus," *Physics of Plasmas*, vol. 29, p. 083508, 08 2022.

[18] S. Lee and A. Serban, "Dimensions and lifetime of the plasma focus pinch," *IEEE Transactions on Plasma Science*, vol. 24, no. 3, pp. 1101–1105, 1996.

[19] P. J. Hart, "Modified Snowplow Model for Coaxial Plasma Accelerators," *Journal of Applied Physics*, vol. 35, pp. 3425–3431, 12 1964.

[20] D. L. Willenborg and C. D. Hendricks, "Design and construction of a dense plasma focus device. final report (part 1)," 10 1976.

[21] S. Auluck, P. Kubes, M. Paduch, M. J. Sadowski, V. I. Krauz, S. Lee, L. Soto, M. Scholz, R. Miklaszewski, H. Schmidt, A. Blagoev, M. Samuelli, Y. S. Seng, S. V. Springham, A. Talebitaher, C. Pavez, M. Akel, S. L. Yap, R. Verma, K. Kolacek, P. L. C. Keat, R. S. Rawat, A. Abdou, G. Zhang, and T. Laas, "Update on the scientific status of the plasma focus," *Plasma*, vol. 4, no. 3, pp. 450–669, 2021.

[22] L. S. Chen Y.H *Int. J. Elect., 35, 341*, 1973.

[23] A. S. S. Lee *IEEE Trans. Plasma Sci*, vol. 24, no. 3, p. 1101, 1996.

[24] V. Oreshkin, "Radiative collapse in z-pinches," *Russ Phys J 40, 1185–1191*, 1997.

[25] B. Appelbe and J. Chittenden, "Understanding neutron production in the deuterium dense plasma focus," *AIP Conference Proceedings*, vol. 1639, pp. 9–14, 12 2014.

[26] L. Soto, C. Pavez, A. Tarifeño, J. Moreno, and F. Veloso, "Studies on scalability and scaling laws for the plasma focus: similarities and differences in devices from 1mj to 0.1j*," *Plasma Sources Science and Technology*, vol. 19, p. 055017, sep 2010.

[27] L. Soto, P. Silva, J. Moreno, M. Zambra, W. Kies, R. E. Mayer, A. Clausse, L. Altamirano, C. Pavez, and L. Huerta, "Demonstration of neutron production in a table-top pinch plasma focus device operating at only tens of joules," *Journal of Physics D: Applied Physics*, vol. 41, p. 205215, oct 2008.

[28] D. Lowe and C. Hagen, "The nstec dense plasma focus laboratories - an overview,"

[29] S. Lee and S. H. Saw, "Numerical experiments providing new insights into plasma focus fusion devices," *Energies*, vol. 3, no. 4, pp. 711–737, 2010.

[30] M. J. Sadowski and M. Scholz, "Plasma dynamics and plasma wall interaction progress in large-scale plasma-focus experiments," 2005.

[31] P. S. Nukulin, V.Y., "Saturation of the neutron yield from megajoule plasma focus facilities," *Plasma Phys. Rep. 33*, 2007.

[32] F. D. McDaniel, B. L. Freeman, and C. M. Fowler, "Applications of a neutron-producing dense plasma focus," in *International Conference Neutrons in Research and Industry* (G. Vourvopoulos, ed.), vol. 2867, pp. 517 – 520, International Society for Optics and Photonics, SPIE, 1997.

[33] A. Patran, L. C. Tan, D. Stoenescu, M. S. Rafique, R. S. Rawat, S. V. Springham, T. L. Tan, P. Lee, M. Zakaullah, and S. Lee, "Spectral study of the electron beam emitted from a 3 kj plasma focus," *Plasma Sources Science and Technology*, vol. 14, p. 549, jun 2005.

[34] S. Springham, R. Verma, M. Zaw, R. Rawat, P. Lee, A. Talebitaher, and J. Ang, "Plasma focus neutron energy and anisotropy measurements using zirconium–beryllium pair activation detectors," *Nuclear Instruments and Methods in Physics Research Section A: Accelerators, Spectrometers, Detectors and Associated Equipment*, vol. 988, p. 164830, 2021.

[35] Z. Pan, R. Rawat, R. Verma, J. Lin, H. Yan, R. Ramanujan, P. Lee, S. Springham, and T. Tan, "Miniature plasma focus as a novel device for synthesis of soft magnetic feco thin films," *Physics Letters A*, vol. 374, no. 8, pp. 1043–1048, 2010.

[36] H. Heo and D. K. Park, "Correlations between argon ion beams and x-rays in a plasma focus," *Japanese Journal of Applied Physics*, vol. 41, p. 3120, may 2002.

[37] A. Shyam and R. K. Rout, "Enhancement of neutron emission from a plasma focus nuclear fusion device by the use of anode with low spark erosion," *Physica Scripta*, vol. 57, p. 290, feb 1998.

[38] M. J. Hogan, C. D. Barnes, C. E. Clayton, F. J. Decker, S. Deng, P. Emma, C. Huang, R. H. Iverson, D. K. Johnson, C. Joshi, T. Katsouleas, P. Krejcik, W. Lu, K. A. Marsh, W. B. Mori, P. Muggli, C. L. O'Connell, E. Oz, R. H. Siemann, and D. Walz, "Multi-gev energy gain in a plasma-wakefield accelerator," *Phys. Rev. Lett.*, vol. 95, p. 054802, Jul 2005.

[39] S. Lee, "Plasma focus radiative model: Review of the lee model code," *J Fusion Energ 33, 319–335*, 2014.

[40] C. Moreno, H. Bruzzone, J. Martinez, and A. Clausse, "Conceptual engineering of plasma-focus thermonuclear pulsors," *IEEE Transactions on Plasma Science*, vol. 28, no. 5, pp. 1735–1741, 2000.

[41] M. A. Liberman, J. S. De Groot, A. Toor, and R. B. Spielman, *Stability of Z-Pinch Plasmas*, pp. 96–132. New York, NY: Springer New York, 1999.

[42] A. Clausse, L. Soto, and A. Tarifeño-Saldivia, "Influence of the anode length on the neutron emission of a 50 j plasma focus: Modeling and experiment," *IEEE Transactions on Plasma Science*, vol. 43, no. 2, pp. 629–636, 2015.